



Effects of grain morphology on suffusion susceptibility of cohesionless soils

M. Ali Maroof¹ · Ahmad Mahboubi¹ · Ali Noorzad¹

Received: 9 July 2020 / Accepted: 28 November 2020 / Published online: 14 January 2021
© Springer-Verlag GmbH Germany, part of Springer Nature 2021

Abstract

Transporting finer fractions inside the soil skeleton or the erosion of base soils within the filter are the two main challenges for earthen hydraulic structures, their foundations, and filter design. Soil particle morphology could influence pore size distribution and transport of fine grains; however, there is not sufficient knowledge on the effect of grain shape on internal erosion. Some experiments designed and conducted in the present study to evaluate the suffusion potential of aggregates with various shapes and different gradations. Particles with six types of grain morphologies and five gradations were collected, and 26 tests were performed. Furthermore, using 3D image processing and visual comparison, particle shape assessed in terms of three features, including sphericity, roundness, and roughness. Results indicated that particle shape influences flow rate, washed-out fine grains in permeameter wall, vertical strain, and mass loss. An increase in the sphericity and roundness causes an increase in the loss of fine grains, pipe in cell sidewall, and vertical strain. Concerning the particle regularity as an indicator of grain morphology, it was demonstrated that the grains with lower regularity are more resistant to suffusion, and thus the resistance to suffusion would decrease with particle regularity. Spherical glass bead and rounded/medium sphericity specimens were more prone to suffusion at an equivalent or even lower hydraulic gradient than the soil samples with angular/low sphericity grains.

Keywords Internal instability · Suffusion · Suffusion/volume change · Particle shape · Grain morphology · Sphericity · Roundness · Roughness · Regularity

Notations

d_x	Particle size that X percent is finer than it
D	Sieve size (mm)
C_c	Curvature coefficient
C_U	Uniformity coefficient
$\frac{D_{15}}{d'_{85}}$	Filter ratio of the components
$\frac{D_{15}}{d'_{85}}$	Grain size corresponding to 85% finer in the finer fraction
D'_{15}	Grain size corresponding to 15% finer in the coarser fraction
F	Percentage smaller than D, mass passing
H	Mass percentage between size D and 4D, mass increment
G_r	Gap ratio
P	Portion of particles finer than 0.063 mm

d_0	Mean pore diameter
d_1	Minimum diameter of pores
a	Shape coefficient, shape factor
d_{min}	Minimum grain diameter
n	Porosity
D_h	Effective diameter
R	Wadell's roundness
S	Inscribed-circumscribed sphere ratio
d_{i-s}	Diameters of the inscribed sphere
d_{c-s}	Diameters of the circumscribed sphere
ρ	Regularity

1 Introduction

Internal erosion is identified as a major cause of damage and failures of fluvial levees, landslide dams, and embankment dams [1]. Transport of fine particles within an earthen structure or its alluvial foundation by the seepage is one of the mechanisms that initiate the erosion [2]. Soil assemblies contain coarse and fine fractions, forming the soil skeleton; if finer particles can move freely through

✉ Ahmad Mahboubi
a_mahboubi@sbu.ac.ir

¹ Faculty of Civil, Water and Environmental Engineering, Shahid Beheshti University, Tehran, Iran

pores between larger particles, that fabric is an internally unstable grading [3–5].

The silt–sand–gravel mixture, glacial tills, fluvioglacial, and alluvial sediments are prone to internal erosion [6]. Internal erosion in research works is described using three terms: suffusion, suffosion, and suffosion [7, 8]. Even if suffosion seems to be the relevant word from an etymological point of view [7], it is not used by the scientific community.

The detachment of fine particles of internally unstable soil and their transport in the coarse matrix could be non-destructive (suffusion) or result in soil structural collapse leading to the failure of earthen structures (suffosion or suffusion/volume change); in this case, the phenomenon is accompanied by a loss of mass, volumetric strain, and a change in permeability [9–12]. Nevertheless, some researchers have shown that the settlement observed with suffusion can improve the mechanical properties of the material [13]. There might be settlements at the earthen structure scale which are likely to be heterogeneous and can lead to locally developed open cracks. Conversely, suffusion can generate underlying mechanical instability which could lead to the hydraulic failure of soil structures in case of a change in the loading conditions [14].

In the evolution of internal erosion and suffusion, the physical characteristics of the soil structure and hydrodynamic conditions play significant roles. Factors controlling soil structure include particle morphology (particle size distribution, PSD, and particle shape), density, porosity, and constriction size distribution (CSD) [15, 16]. Further, in internally unstable soils, a hydromechanical condition must also be prepared to initiate either the suffusion or suffusion/volume change mechanism [16]. Effective factors in hydrodynamic conditions include seepage velocity, hydraulic

gradient, discharge flow direction, effective surcharge or confinement stresses, and leakage duration [17–21].

The internal stability geometrical criteria can be categorized into two general groups. The first group is a function of the shape of the PSD curve and inspects the probability of filtering the finer portion by coarser one in the soil (self-filtering), and the second group compares the equivalent diameter of the soil pores and diameter of the smallest particle. Most of the proposed methods in the first group are directly or indirectly dependent upon the shape or slope of the particle size distribution curve [7, 18, 22]. Table 1 depicts a set of the common geometrical criteria related to internal stability.

In the second group of geometrical criteria named capillary tube model, the possibility of movement of fine grains within the pores of coarser particles due to the seepage force is studied [23]. Where the mean diameter of pores between coarser fraction (d_0) is less than the minimum grain diameter ($d_0 \leq d_{min}$ and $d_{min} = d_{85}^f$), the grains would not move into an adjacent layer or within the layer [18, 23–26].

The Kovacs criterion [23] considers the influence of the morphological properties via the shape coefficient. The shape coefficient for granular soil is commonly calculated by theoretical formulas or approximated by comparing the grain shape with regular geometric shapes, such as sphere and polyhedron [27]. This factor is suggested to be equal to 6, 7–9, 9–11, and 20, respectively, for spheroid, rounded, angular, and laminated particles [23]. Thus, particle morphology probably has a significant contribution to suffusion [8].

The satisfaction of geometrical, stress, and hydraulic criteria are necessary for the occurrence of suffusion [2]. Geometrical criteria for the assessment of stability are only useful for suffusion susceptibility assessment, and for precise evaluation of suffusion occurrence, there is a need for

Table 1 Common proposed geometrical criteria for internal instability

References	Criteria	Definition
Istomina [28]	$C_u \leq 10$: internally stable $10 \leq C_u \leq 20$: transition zone $C_u \geq 20$: internally unstable	C_u : uniformity coefficient
Kezdi [17]	$(d_{15}^c/d_{85}^f)_{max} \leq 4$: internally stable	d_{15}^c : particle size corresponding to 15% smaller in the coarser fraction d_{85}^f : 85th percentile of particle size in the finer fraction
Kenney and Lau [29]	$(H/F)_{min} \geq 1.0$: internally stable	F : percentage smaller than arbitrary D H : mass increment between size D and $4D$
Burenkova [30]	$0.76 \log(h'') + 1 < h' < 1.68 \log(h'') + 1$: internally stable	$h'' = d_{90}/d_{15}$, $h' = d_{90}/d_{60}$
Wan and Fell [18]	$30/\log(d_{90}/d_{60}) < 80$, or $30/\log(d_{90}/d_{60}) < 80$ and $15/\log(d_{20}/d_5) > 22$ internally stable	
Chang and Zhang [31]	$P < 10$ $G_r < 3$ $10 < P < 35$ $G_r < 0.3P$ $P > 35$ Stable	P : fines content G_r : gap ratio $G_r = d_{max}/d_{min}$ which d_{max} and d_{min} : maximum and minimum grain diameter in the gap, respectively
Kovacs [23]	$d_0 = \frac{4n}{1-n} \frac{D_h}{\alpha}$ and $d_1 = 2/3 d_0 d_0 \leq d_{min}$ and $d_{min} = d_{85}^f$	d_0 : minimum diameter of pore: shape factor, D_h : effective diameter, n : porosity

performing tests on the soil samples. Onset internal instability occurrence can be divided into two general groups; loss of smaller grains and subsequent phenomena, and the hydromechanical effects, either lonely or collectively. The former might lead to increase in hydraulic conductivity, and change in the local hydraulic gradient.

Seepage-induced mass loss and sample deformation are commonly used to quantify internal instability [9]. There is no specific quantitative technique to determine whether the soil is internally unstable just by considering mass loss or sample deformation [31]. In this regard, there are some considerations presented in the following:

- Visual observations of particle loss, violent piping of fines, or visible mass loss in plexiglas sidewall [18, 32, 33].

The lost mass of fine particles or rate of loss of finer particles, when the criterion is the loss of fine grains exceeding 1 g.m^{-2} per second during fine grains exit [32, 34]. The minimum variation of initial grading curve and grading after test, as fraction flushed out, of internally unstable soils is about 7% in the Kenney and Lau's tests [3]. Skempton and Brogan [32], in one of their experiments, mentioned that the soil with a 5.6% mass loss was unstable. If the mass loss is higher than 3% of the total sample dry mass and filter velocity is continuously increasing without changing the hydraulic gradient, the sample can be evaluated as internally unstable [35]. In the tests conducted by Douglas et al., a sample with a mass loss of more than 5% or between 1% and 5% of the total sample dry mass, but $\geq 10\%$ of the finer fraction dry mass, was classified as major erosion [6]. Further, one of their samples, with the amount of erosion exceeding 2.2% of the total sample mass and more than 8.0% of finer fraction, was categorized as suffusive [6].

Change in sample volume or length, and the limit of about 1.2% deformation in the sample, is used for identifying the unstable soils during internal erosion [36]. Sample deformation equal to 2–5% corresponds to about 8–13% of mass loss in the experiments [37]. This value is 1% in other experiments corresponding to about 4% loss of fine particles, which can be considered the boundary value of washed-out grain to distinguish stable soils from unstable ones [31]. This depends on whether the soil is simply suffusive (seepage-induced mass loss) or suffusive with volume change (deformation/settlement accompanied by mass loss) [9].

Hydromechanical considerations are often measured by hydraulic gradient and flow rate. First, it is presumed that a change in local permeability occurs together with the loss of fine grains [9]. Further, the

flow rate may be used as an indicator of suffusion progress [38]. When the soil permeability increases gradually or rapidly, suffusion happens in the presence of increased permeability, higher seepage velocities, which might accelerate the rate of suffusion [21]. Generally, the findings can be mentioned as below:

- A rapid increment occurs in the seepage velocity at a constant gradient [32].
- The change of local hydraulic gradient values with time [37].
- A change occurs in the net discharge flow weight, at a constant gradient, or variation in discharge-gradient relationship [18].
- Visual observations, qualitatively, with a change of spatial and temporal local hydraulic gradient along the length of the soil sample and from axial deformation during a test, quantitatively, [39].

The physical properties of the soil structure and hydrodynamic conditions are the factors governing internal stability. Few studies have investigated the influence of grain morphology on suffusion, and it appears that there is no clear conclusion regarding the effect of particle morphology either in internal instability criteria or in the results of experiments performed to ascertain suffusion potential [8, 40]. In capillary tube models [23, 41–43], the shape factor is used to estimate the equivalent diameter of pores by empirical equations. This is due to the fact that an increase in the angularity of particles increases the shape factor and decreases the mean diameter of pores [8].

Marot et al. (2012) performed suffusion tests on three types of sand with different roundness. They investigated the effect of grain angularity on grains' erosion rate. Their results indicated that an increase in the grain angularity caused a reduction in hydraulic conductivity and an increase in the suffusion resistance [44].

Further, some studies have been performed on glass bead and sandy soils [33, 40, 45–47]. A study of four paired-tests on glass bead and sub-angular sand was reported [45]. Their test results demonstrated that the spherical glass bead specimens are more susceptible to suffusion/volume change than the companion of sub-angular soil specimens. Consequently, particle shape is a factor governing the prone to suffusion/volume change and should be pondered when studying this phenomenon [45].

In the current research, the effect of grain morphology on the suffusion susceptibility of soil samples was studied. Samples with six different shapes and five different particle size distribution curves were prepared and under a downward flow, and a stepwise hydraulic gradient were performed.

2 Material

2.1 Sample gradation

In order to study the particle morphology effect on suffusion, experiments were carried out on internally stable, transitional, and internally unstable soils. All samples were made from two materials: glass bead with a glassy and rough texture and four soil particles with different shapes, including crushed, natural alluvial grain; and residual soils. Further, five different grain size distributions were considered to study the effect of PSD. Therefore, a total of 26 samples were prepared and tested. These soil gradations consisted of a widely distributed, two upward concave gradations, and two gap-graded gradations. Selected PSD curves included:

- K gradation, a widely distributed, upward concave, and internally stable grading [3]. The K gradation has already been studied and is an internally stable, widely distributed grading. Experiments were performed on sandy gravels in an apparatus with 125 mm diameter, and results showed no change in the gradation after the test [3].
- In order to investigate the effect of grain shape on internal instability of gap graded soils, the test was performed on two gradations with different gap ratios (Gr), G3-13 [48, 49], and GP-1 grading. Gap ratios of G3-13 and GP-1 grading were equal to 10 and 6.7, respectively. The portion of particles finer than 0.063 mm, P, was less than 10%, and these soils were unstable for $Gr > 3$ [31].
- B gradation, an upward concave grading with a stable transitional zone predicted as internally stable by some criteria and judged as internally unstable according to

other criteria [32]. The B gradation is a widely distributed grading with about 15% finer fraction, $(H/F)_{\min} = 0.98$, a filter ratio of components $D'_{15}/d'_{85} = 3.7$, and a uniformity coefficient of $C_u = 9.7$. B gradation seemed to lie on a boundary between internal stability and instability. Nevertheless, with 37% of porosity, the specimen had a low relative density, and the experimental results showed that it is definitely unstable [32].

- M1, an upward concave, and potentially internal unstable grading (see Table 3). The coarse fraction in M1 gradation was similar to that of B gradation but with a flatter slope in finer fraction.

PSD curves of particles are shown in Fig. 1, and the gradation characteristics of each group are given in Table 2. The summary of internal stability/instability classification with proposed criteria is presented in Table 3.

2.2 Particle shape

The effect of grain shape on suffusion susceptibility was studied by selecting five different shapes with different geological and morphological properties.

Three distinct features can describe particle shape from macro to micro scales, including sphericity, roundness, and roughness [50–53]. Besides, flatness and elongation ratio can be used to describe the overall particle form [54].

Herein, particle sphericity (S), was measured using the 3D digitized particles from X-ray micro-computed tomography images.

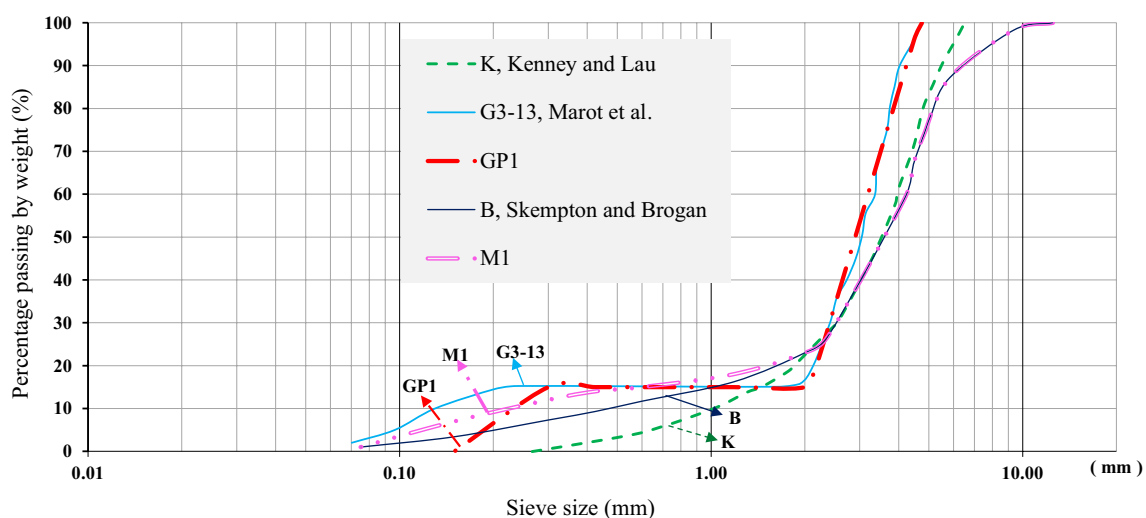


Fig. 1 The particle size distribution of test materials

$$S = \frac{d_{i-s}}{d_{c-s}} \tag{1}$$

In which d_{i-s} and d_{c-s} are the inscribed sphere diameter and circumscribed sphere diameter, respectively. Particle sphericity class is assigned to the spherical (equant) and ellipsoid (elongated) particles (see Table 4), as suggested by Maroof et al. [55].

For all soil samples, The mean values of Wadell’s roundness [56], R , were measured and classified by the verbal scale proposed by Powers [57]. Further, surface roughness is classified visually under six textural groups: very rough, rough, relatively rough, corroded, smooth, and glassy [55]. For flaky and elongated particles, flatness and elongation ratio were also measured. Table 4 indicates the number of

particles analyzed for each grain shape concerning the classification/ description of particle shape.

Fig. 2 illustrates photographs of coarser fraction and finer fraction for six types of particles. Besides, Fig. 3 depicts SEM images of finer fraction for glass bead, rounded, crushed, flaky, and elongated grains.

3 Experiments

3.1 Apparatus setup

Internal stability was assessed by the suffusion permeameter device, as diagrammatically illustrated in Fig. 4. Similar devices have also been used by other researchers, [3, 6, 12,

Table 2 Characteristics of test gradations

Material	PSD	D_5	D_{10}	D_{30}	D_{60}	D_{90}	C_u	C_c
Glass bead, Soil	K	0.62	1.06	2.57	3.98	5.55	3.76	1.57
Glass bead, Soil	G3-13	0.10	0.13	2.41	3.36	3.99	25.4	13.3
Glass bead, Soil	GP-1	0.20	0.29	2.41	3.36	3.99	11.6	5.96
Glass bead [†] , Soil	B	0.21	0.45	2.61	4.38	6.34	9.73	3.46
Glass bead, Soil	M1	0.15	0.21	2.61	4.38	6.34	20.8	7.58

[†]Glass bead with glassy surface and rough texture

Table 3 Summary of internal stability/instability classification with proposed criteria

PSD	Istomina[28]	Kezdi[17]	Kenny & Lau[29]	Bouren-cova[38]	Wan and Fell[18]	Li & Fan-nin[9]	Chang and Zhang[31]
K	S	S	S	S	T	S	S
B	S	S	T	U	T	U	T
M1	U	U	U	U	U	U	U
GP-1	T	U	U	U	T	U	U
G3-13	U	U	U	U	U	U	U

S: stable, U: unstable, T: transient

Table 4 Particle shape classification/description

Particles	S	Sphericity class	Elongation ratio	Flatness ratio	Wadell’s roundness	Roundness class	Roughness [†]	The average number of measured particles
Glass bead	0.99	High sphericity	–	–	0.99	Well rounded	Glassy‡	1
Rounded alluvial	0.46	Medium sphericity	–	–	0.65	Rounded	Relatively smooth	30
Crushed aggregate	0.39	Low sphericity	–	–	0.15	Very Angular	Rough	36
Slate	0.13	Slab	–	0.17	0.46	SubRounded	Relatively smooth	38
Weathered pyramid basalt	0.096	Elongated	0.19	–	0.18	Angular	Relatively rough	25

[†] Attained qualitatively based on the visual comparisons, [‡] Suffusion tests on the B grading were performed on glassy and rough glass beads

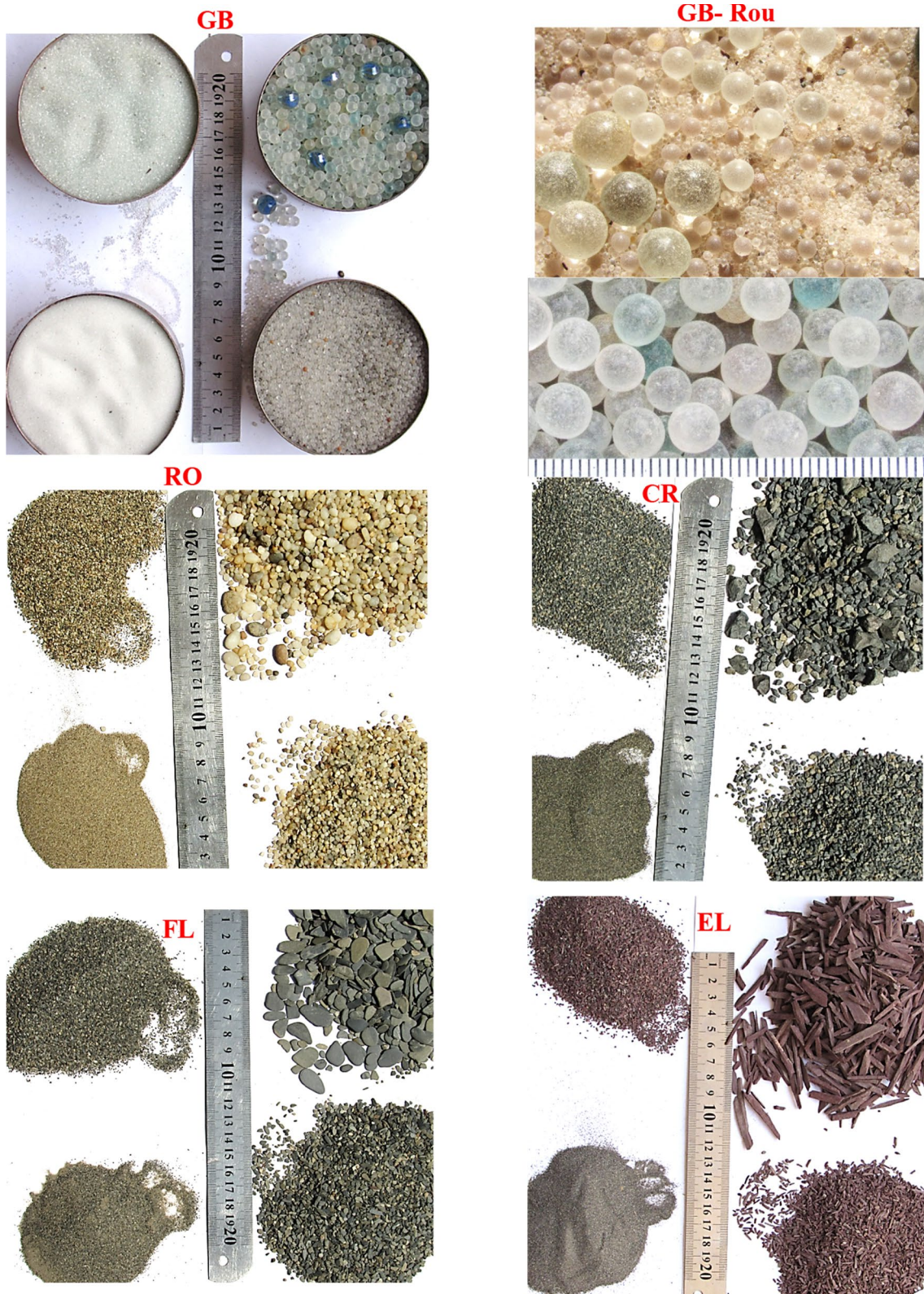


Fig. 2 Images of coarser fraction and finer fraction. GB: glass bead, GB-Rou: rough glass bead, RO: rounded particle, CR: crushed aggregates, EL: elongated particle, FL: flaky particle

Fig. 3 SEM image of finer fraction particles: GB: glass bead, RO: rounded particle, CR: crushed aggregates, EL: elongated particle, FL: flaky particle

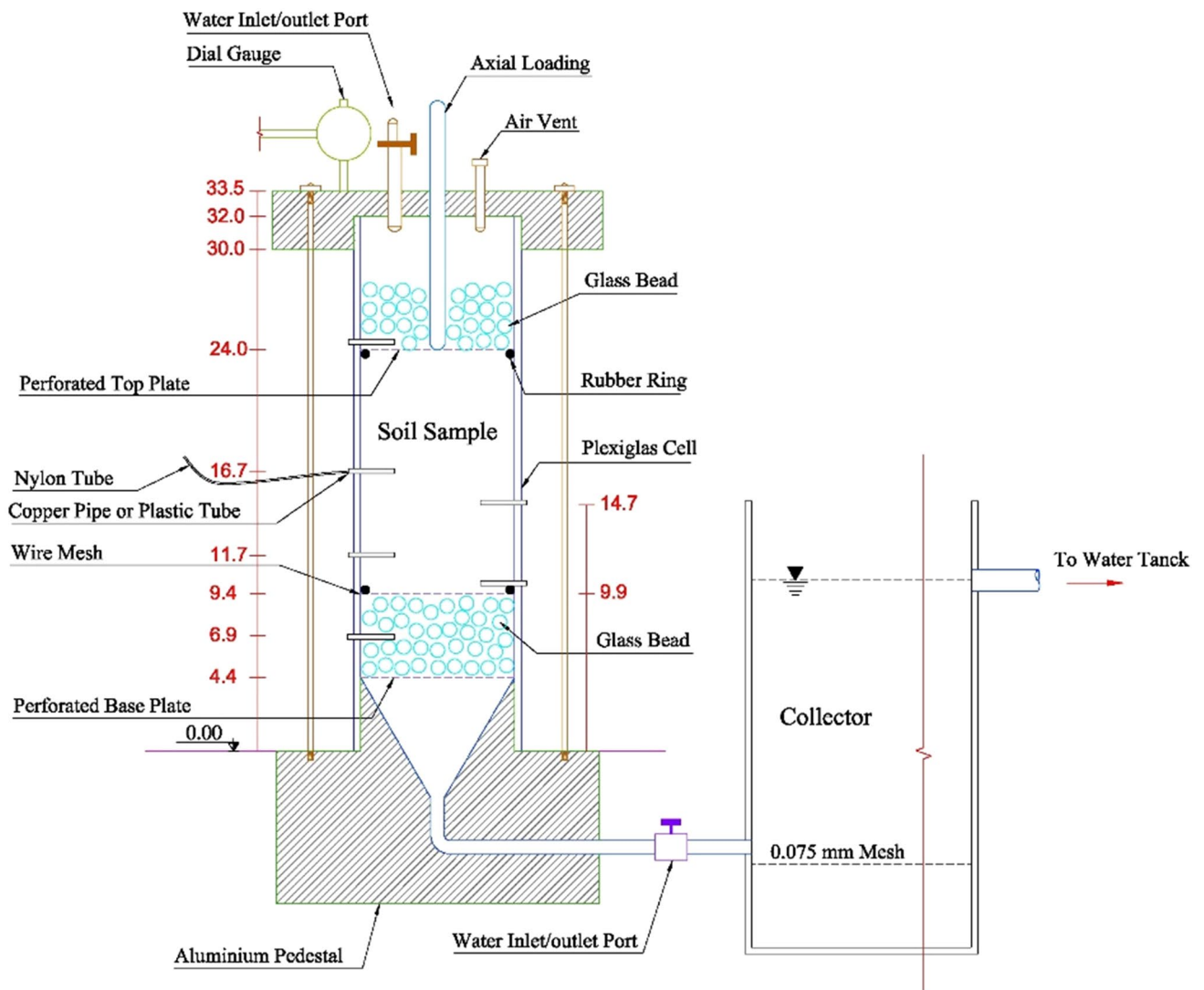
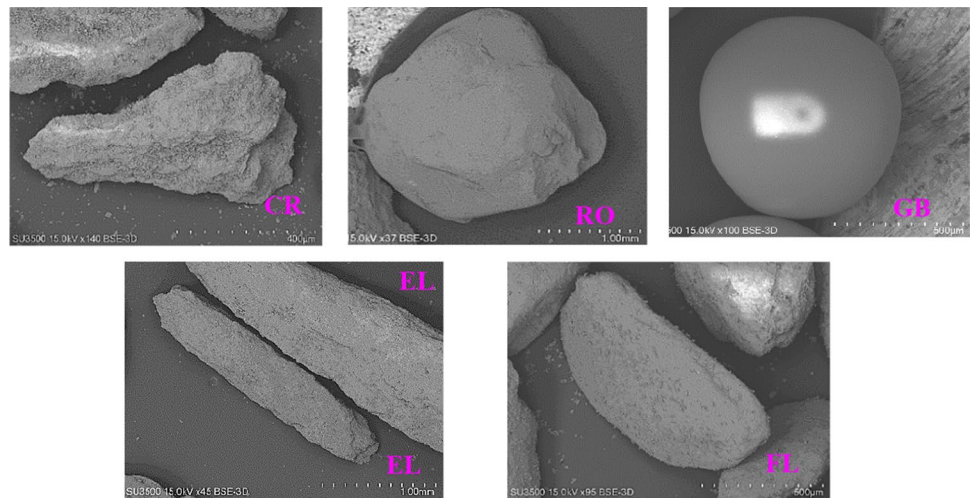


Fig. 4 Test apparatus

58], and devices that are able to impose a pre-stress [32, 47, 59, 60].

The permeameter is typically a plexiglas cell with an internal diameter of 91 mm and a height of 340 mm. The sample was located on a wire mesh screen that was placed on 10 mm diameter glass beads. Mesh size was selected so as allow the erosion of finer fraction and act as a filter for coarser fractions to remain in place. In this way, the overall structure of the soil would be preserved. Exit wire mesh with opening sizes of either 2.0 mm (soil types K and G3-13) or 1.18 mm (soil types B, M1, and GP-1) was used. The drainage layer at the top of the seepage cell consists of a 10 mm mono-size glass bead, supported with a perforated top plate.

The apparatus was able to perform the test in two states of downward and upward seepage flow and applying vertical stress under oedometric conditions. The funnel-shaped bottom of the device facilitates eroded grains collection. Glass bead layer on top of the sample causes a uniform flow to the sample surface [61]. Wire mesh at the bottom of the specimen was supported by a 15 mm glass bead layer, and the water level could be measured by the piezometer installed at the bottom of the sample. The gradient could be measured at different levels using copper or plastic tubes along with the sample height.

3.2 Sample preparation and test method

Concerning the possibility of segregation of grains and the movement of finer fraction within the pores during sample preparation; the samples were prepared using the moist tamping technique. Water was added to the soil samples with moisture content up to 3–7%. The samples were prepared in three layers that had a thickness of about 45 mm each and were compacted using a tamping rod to reach the relative density of 52–58%. After installation of the samples with medium density, a surcharge load equal to 25 kPa was gradually applied to the sample to allow settlement and formation of likely changes in the soil grains arrangement. The presence of this surcharge preserves effective positive stress inside the primary fabric [29].

Then, de-aired water enters the sample under a small head, and the sample percolates slowly upwards to recover the falling grains in the funnel-shaped area and also, reducing movement of the fine grains during specimen saturation. Reaching the water to the piezometer tube level, first, a plastic or copper pipe is inserted about 2 cm into the samples as suggested in [61]. After the water flows through the pipe, it is connected to a nylon tube linked to a glass piezometer. Water head upstream, downstream, and along the sample is measured using installed water piezometer outlets.

It has been known that in internally unstable soils, initiation of suffusion is dependent on the hydraulic gradient [62]. Under a multi-stage hydraulic gradient, the amount

of erosion is affected by the applied hydraulic gradient and time of each step. Furthermore, two conditions are necessary to perform a suffusion test: stabilization of hydraulic conductivity and providing erosion process [48, 63]. Thus, samples are subjected to downward seepage flow with a constant head and multi-stage hydraulic gradients varying from 0.15 to 8.0. The test duration per gradient is variable from 30 min to 3 h. For each gradient, the test was stopped after a lack of observing erosion of the grains and also observing a constant discharge flow and no changes in the hydraulic gradient.

The vertical strain was calculated by measured vertical deformation of the sample. Eroded particles from the samples at the end of each applied gradient were collected on the 0.075 mm mesh at the downstream basin. After the test, each sample was divided into three layers with predefined height, and each layer portion was re-graded.

4 Results

Suffusion and suffusion/volume change are described by seepage-induced loss of fine particles, reduction in volume, and variation of permeability. In the current study, mass loss, vertical strain, and change in flow rate were reported. Furthermore, visible migration of fine particles through the wall of the permeameter can be utilized to qualitatively describe the occurrence of internal instability.

4.1 Visual observation

Visual observations were used to describe the occurrence of fine migration through the wall of the plexiglas during the tests and after each applied hydraulic gradient.

The time that washes out of fine particles was observed since the start of fine erosion and the total test duration presented in Table 5. Often, finer fraction erosion was observed temporarily after each increase in the gradient. In internal stable and transient samples (K and B) the erosion time, since the start of fine erosion increases in a higher hydraulic gradient. Nevertheless, in the internally unstable sample (M1, G3-13, and GP-1), the suffused time was greater for low hydraulic gradients and was reduced for $i_{av} = 3.0$ and $i_{av} = 8.0$.

Moreover, the internal instability occurrence is demonstrated qualitatively. Visual descriptions of particle movement at each stage were recorded. Fine-grain washed-out indications at the plexiglas sidewall were: localized erosion, multiple localized erosion, and broken and/or straight pipe through the wall of the permeameter, which was assigned to the low, moderate, and high grades, respectively.

The pipes extended as broken lines have a variable direction in the direction of the flow. The near straight pipes along

Table 5 Suffused time, since the start of fine erosion (min) and the total test duration (min)

<i>PSD</i>	<i>i_{av}</i> or ($\Delta h/l$)	<i>i_{av}</i> =0.15	<i>i_{av}</i> =1	<i>i_{av}</i> =3	<i>i_{av}</i> =8	Total test duration (min)
<i>K</i>	<i>GB</i>	7	No sign	25	30	330
	<i>SR</i>	10	No sign	No sign	30	285
	<i>A</i>	15	No sign	10	15	300
	<i>F</i>	10	No sign	5	15	300
	<i>E</i>	5	No sign	5	20	240
<i>B</i>	<i>GB</i>	15	45	15	5	330
	<i>GB-Rou</i>	No sign	12	17	10	205
	<i>SR</i>	10	40	25	12	310
	<i>A</i>	20	45	50	20	330
	<i>F</i>	10	15	20	10	300
<i>M1</i>	<i>E</i>	10	15	10	10	300
	<i>GB</i>	25	75	20	15	270
	<i>SR</i>	15	70	45	12	290
	<i>A</i>	No sign	60	15	7	205
	<i>F</i>	No sign	80	30	10	255
<i>GP-1</i>	<i>E</i>	7	15	10	5	195
	<i>GB</i>	110	36	22	14	330
	<i>S-R</i>	94	55	21	15	330
	<i>A</i>	60	42	25	10	300
	<i>F</i>	55	58	17	20	270
<i>G13</i>	<i>E</i>	45	16	10	12	300
	<i>GB</i>	60	45	20	10	270
	<i>SR</i>	55	40	30	10	330
	<i>A</i>	75	30	27	10	390
	<i>F</i>	90	30	45	15	480
	<i>E</i>	40	20	15	10	270

GB: Glass bead, GB-Rou: Rough glass bead, R: Rounded particle, A: Angular (Crushed aggregate), F: Flaky (Slate), E: Elongated (Weathered pyramid basalt)

with the height of the permeameter cell might be a sign of the development of a ‘pipe’ inside the soil structure and formation of relatively free pathways for water and finer fraction as concentrated channels. Visual observation of fine erosion is given in Table 6.

Some samples such as K, B, and M1 at low hydraulic gradient only show slight changes in the cell wall. Images of sample B at the end of the tests with $i_{av} = 8.0$ are presented in Fig. 5. In this images the erosion paths (erosion zones) are indicated with yellow lines. In glass bead and rounded grains samples, mass loss of fine grains on the sidewall of the plexi-glas cell was found to be relatively high, like a broken pipe. In the sample with flaky grain, mass loss of finer fraction at the cell wall was intermediate, and for crushed and elongated grains, localized erosion was observed through the cell wall.

4.2 Hydrodynamic condition

The suffusion phenomenon results in changes in discharge flow and hydraulic gradients. The erosion rate of the fine

grains, discharge flow rate, and hydraulic gradient was measured for each applied hydraulic gradient. The discharge flow was typically measured a few minutes after the increase of each head, during the tests, and before the next steps. The average specific discharge flow (cm/s) at the start and finish of each step, the maximum erosion rate from visual observation, and the test results with downward flows are given in Table 7.

It was observed that the flow rate increased for the case of the glass bead and rounded samples of GP1 and G3-13 throughout the constant $i_{av} = 0.15$. The results showed different discharge flow in other applied hydraulic gradient at the start and finish of each step. Therefore, the migration of fine grains within the specimen may cause either clogging the pores or enlarge preferential channels and may be fine grains transported in flow direction and deposited or trapped in the downstream layer. The decrease in discharge flow and fine erosion may be attributed to the filtration process of the fine grains causing clogged constrictions, as prior have been discussed [7, 8, 64, 65].

Table 6 Plexiglas side wall visual observation

PSD	Particle shape	Observation of fine erosion in the plexiglas sidewall			
		$i_{av}=0.15$	$i_{av}=1.0$	$i_{av}=3.0$	$i_{av}=8.0$
K	GB	No sign	No sign	No sign	Moderate
	SR	No sign	No sign	Moderate	Relatively High [‡]
	A	No sign	No sign	No sign	No sign
	F	No sign	No sign	Moderate	Moderate [‡]
	E	No sign	No sign	No sign	Moderate
B	GB	Moderate	Moderate	High* [‡]	High* [‡]
	GB-Rou	Low	Low	Moderate	Moderate [‡]
	SR	Moderate	Moderate	High* [‡]	High* [‡]
	A	Low	Moderate	Moderate	Moderate [‡]
	F	Low	Moderate	Moderate	High* [‡]
M1	GB	Moderate	High*	High* [‡]	High* [‡]
	SR	Low	Moderate	High*	High*
	A	Low	Moderate	High* [‡]	High* [‡]
	F	Moderate	Moderate	High* [‡]	High* [‡]
	E	Low	Low	Moderate [‡]	High* [‡]
GP-1	GB	High*	High*	High* ^{†,‡}	High* ^{†,‡}
	S-R	Moderate	High* [‡]	High* ^{†,‡}	High* ^{†,‡}
	A	Low	Moderate	High*	High*
	F	Moderate	High*	High*	High* [†]
	E	Low	Moderate	High* [‡]	High* [‡]
G13	GB	Moderate	Moderate	High* [‡]	High* ^{†,‡}
	SR	Moderate	Moderate	High* [‡]	High* ^{†,‡}
	A	Moderate	Moderate	High* [‡]	High* [‡]
	F	Moderate	High*	High*	High*
	E	Moderate	Moderate	Moderate [‡]	High* [‡]

*BL: Broken Line, †SL: Straight Line, ‡partially accumulate by a layer of fines against the wire mesh

The B gradation experiment showed that fraction loss of glass bead sample was measured at an average rate of 2.65 g.m⁻².s⁻¹ in about 15 min since the start of fine erosion at $i_{av}=3$. This value was measured for the sample with rounded grain 2.61 g.m⁻².s⁻¹ in about 12 min since the start of fine erosion at $i_{av}=8$, which is in agreement with the results of Skempton and Brogan’s test, 2.5 g.m⁻².s⁻¹, since the start of slight local piping.

4.3 Mass loss

Washed away particles of the specimens at the end of each applied hydraulic gradient were collected, and the percentage weight of loss mass to the initial dry weight was measured. These values present particles that moved through the specimen and migrated to the outlet.

4.3.1 K Gradation

In the current tests, K gradation samples were made with four types of grain and glass beads. For the gradient of 0.15, a small number of grains were eroded, while for the case of the gradient of 1.0, no fraction loss of fine grains has occurred. Fine-grain movement may have occurred partly during the sample preparation or sample saturation, as reported in previous researches [21, 47].

By increasing the gradient to 3 and 8, the rate of eroded grains increased (Fig. 6). The highest amount of dry mass loss is related to the glass bead sample, followed by rounded particles.

4.3.2 B Gradation

The B gradation has already been studied [32]. In the performed experiments by Skempton and Brogan, the shape of soil grains was subangular, with moderately high sphericity. The amount of eroded grains for sample B comprised 12% finer fraction, which was about 1.8% of the total sample mass. The amount of washed out fines is compatible with the test performed on the sample with rounded to subrounded grains in the present study (Fig. 7).

Moreover, another test was performed on the rough-textured spherical glass bead to separately estimate the effect of the overall form and roughness, the results of which indicated that the surface texture also affects the susceptibility to particle migration, especially in the low hydraulic gradients (see Fig. 7).

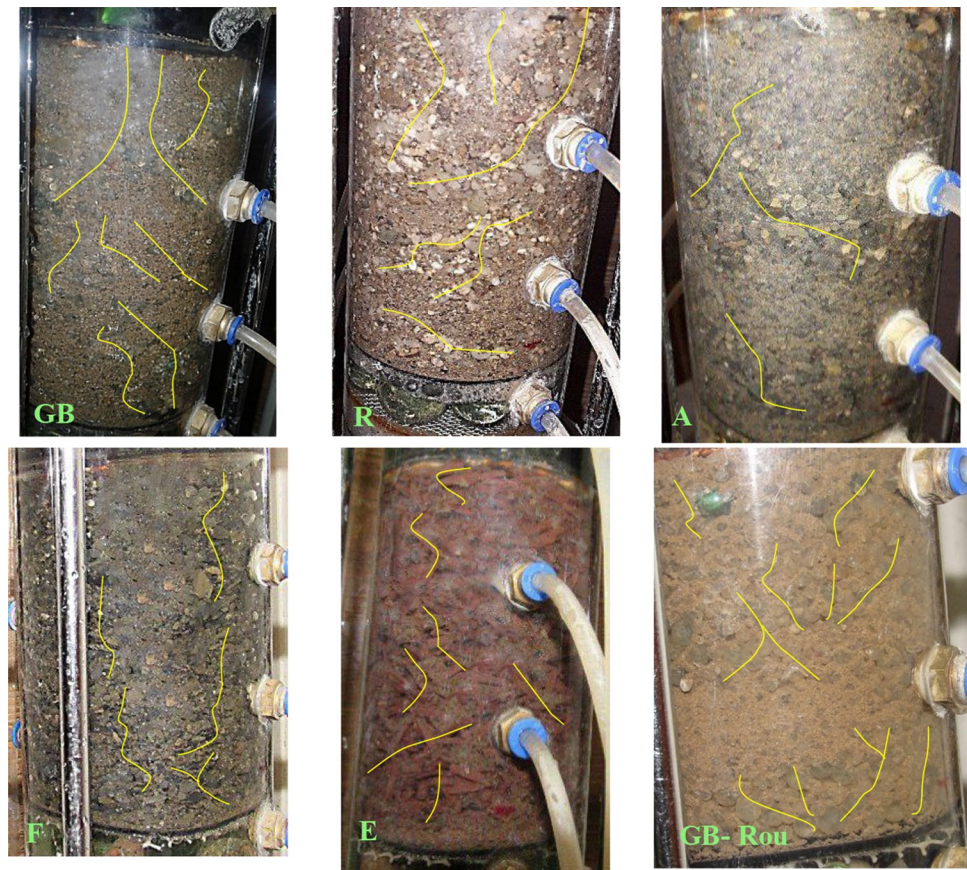
4.3.3 M1 Gradation

The fraction loss in M1 gradation was similar to that of B gradation in $i_{av}=0.15$. Test results showed the minor movement of grains at relatively low gradients, but the main movements were observed at higher gradients of 1 and 3 (Fig. 8).

4.3.4 G3-13 Gradation

The G3-13 gradation is a gap graded soils with gap ratios equal to 10. The exit of finer fraction grains of the glass bead sample at a gradient of 0.15 was about 6% of the total sample weight, and it is internally unstable at this gradient (Fig. 9). The maximum mass loss measured for this sample was 10.01% of the total sample mass, and the maximum deformation was recorded for this sample with a 2.9% vertical strain (see Table 8).

Fig. 5 Images of B grading with different grain shapes, GB: Glass bead, GB- Rou: rough glass bead, R: rounded, A: angular, F: flaky, and E: elongated particles, at the end of the tests



4.3.5 GP-1 Gradation

GP-1 gradation is also a gap graded soil where its coarser fraction is similar to that of G3-13 gradation, and its finer fraction is coarser. Its gap ratio is equal to 6.67. Mass loss in the glass bead and rounded sample at a gradient of 0.15 exceeds 3.0% of the initial sample weight, and these were internally unstable at this gradient.

5 Summary and discussion

5.1 Summary

In the current study, suffusion, suffusion/volume change, and initiation of internal instability are judged based on one or a group of manifestations; visual observations, qualitatively, mass loss, erosion rate, and vertical strain, quantitatively.

Due to the shortcomings of quantitative technique for the soils' internal stability/instability determination, quantitative/qualitative terms have been chosen and adopted in this research based on previous suggestions [6, 29, 31–33, 39].

The internal erosion process is described by the term “suffusion” if just mass loss takes place, and the term would be used “suffusion/volume change” in case the mass

loss is accompanied by volumetric change or the observation of straight pipe in the plexiglas sidewall. The samples with mass loss of higher than 3% of the initial sample dry mass were categorized as suffusive, and samples with mass loss effect on plexiglas wall, like a broken line in cell sidewall, during the tests and/or mass erosion rate exceeds $2.0 \text{ g} \cdot \text{m}^{-2} \cdot \text{s}^{-1}$, were classified as transient. Further, samples with a vertical strain of more than 1.0% were considered as suffusive/volume change. Samples with a straight pipe in the sidewall and a vertical strain less than 1.0% were classified as transient.

The amounts of eroded mass regarding the total sample weight of glass bead, rounded, crushed, flaky, and elongated particles are presented in Fig. 10. The experimental results indicate two visible effects, including the particle shape and the particle size distribution (particle morphology). The percentage of eroded particles relative to the total sample weight increased with sphericity and roundness. Moreover, test results indicated that increasing the coefficient uniformity (C_u) resulted in more significant mass loss. Besides, the effect of grain shape was more considerable for gap-graded soil. In the gap-graded soil, GP-1, and G3-13, the difference between mass loss percentages increased (Fig. 10-(b)). The peak in the diagram of Fig. 10-(b) corresponds to GP-1 gradation, which is a gap-graded soil. For the other used

Table 7 Specific discharge flow (cm/s) at the start and end of each step and maximum erosion rate at i_{av} ($\text{g}\cdot\text{m}^{-2}\cdot\text{s}^{-1}$)

PSD	Particle type/shape	Max. erosion rate at (i_{av})	Start or end of the steps	$i_{av}=0.15$	$i_{av}=1$	$i_{av}=3$	$i_{av}=8$	
K	Glass bead	1.91 ($i=0.15$)	start	0.21	0.44	0.51	1.27	
			end	0.22	0.45	0.50	1.23	
	Sub rounded	0.51 ($i=0.15$)	start	0.15	0.39	0.52	1.20	
			end	0.15	0.37	0.52	1.21	
	Angular	0.14 ($i=0.15$)	start	0.24	0.54	0.73	1.36	
			end	0.24	0.53	0.73	1.31	
	Flaky	0.12 ($i=8.0$)	start	0.19	0.44	0.69	1.17	
			end	0.20	0.46	0.66	1.14	
	Elongated	0.53 ($i=0.15$)	start	0.32	0.47	0.63	1.57	
			end	0.32	0.48	0.60	1.51	
	B	Glass Bead	3.71 ($i=8.0$)	start	0.09	0.31	0.40	0.76
				end	0.08	0.32	0.40	0.76
Rough glass bead		2.59 ($i=8.0$)	start	0.08	0.31	0.42	0.73	
			end	0.08	0.29	0.40	0.72	
Sub Rounded		2.61 ($i=8.0$)	start	0.09	0.27	0.41	0.69	
			end	0.08	0.26	0.39	0.67	
Angular		0.60 ($i=1.0$)	start	0.16	0.37	0.48	0.81	
			end	0.12	0.37	0.47	0.78	
Flaky		1.43 ($i=8.0$)	start	0.14	0.37	0.51	0.82	
			end	0.13	0.38	0.51	0.81	
Elongated		0.89 ($i=8.0$)	start	0.17	0.46	0.59	1.14	
			end	0.16	0.47	0.58	1.12	
M1	Glass Bead	2.78 ($i=3.0$)	start	0.12	0.41	0.55	0.88	
			end	0.10	0.44	0.56	0.81	
	Sub Rounded	2.59 ($i=3.0$)	start	0.11	0.34	0.43	0.60	
			end	0.11	0.35	0.44	0.62	
	Angular	3.39 ($i=3.0$)	start	0.11	0.37	0.45	0.57	
			end	0.12	0.35	0.49	0.62	
	Flaky	2.03 ($i=3.0$)	start	0.12	0.39	0.51	0.59	
			end	0.12	0.35	0.50	0.63	
	Elongated	2.13 ($i=8.0$)	start	0.17	0.46	0.60	1.06	
			end	0.17	0.45	0.56	1.01	
	GP-1	Glass Bead	1.71 ($i=1.0$)	start	0.09	0.42	0.59	1.15
				end	0.12	0.45	0.59	1.10
Sub Rounded		2.14 ($i=8.0$)	start	0.10	0.47	0.57	1.03	
			end	0.11	0.47	0.58	1.10	
Angular		3.59 ($i=8.0$)	start	0.13	0.43	0.56	0.84	
			end	0.16	0.45	0.58	0.88	
Flaky		1.81 ($i=8.0$)	start	0.10	0.42	0.55	0.85	
			end	0.10	0.43	0.57	0.87	
Elongated		2.25 ($i=8.0$)	start	0.18	0.48	0.63	1.24	
			end	0.18	0.48	0.63	1.30	

Table 7 (continued)

PSD	Particle type/shape	Max. erosion rate at (i_{av})	Start or end of the steps	$i_{av}=0.15$	$i_{av}=1$	$i_{av}=3$	$i_{av}=8$
G3-13	Glass Bead	3.44 ($i=0.15$)	start	0.13	0.48	0.59	1.29
			end	0.16	0.49	0.63	1.31
	Sub Rounded	3.78 ($i=3.0$)	start	0.12	0.45	0.57	1.11
			end	0.14	0.47	0.58	1.11
	Angular	2.97 ($i=1.0$)	start	0.11	0.49	0.61	1.18
			end	0.12	0.50	0.63	1.13
	Flaky	3.13 ($i=1.0$)	start	0.13	0.44	0.55	0.87
			end	0.13	0.43	0.56	0.93
	Elongated	2.45 ($i=3.0$)	start	0.16	0.50	0.64	1.04
			end	0.17	0.50	0.66	1.06

Fig. 6 Percentage of cumulative fines loss after hydraulic gradient for “K” grading

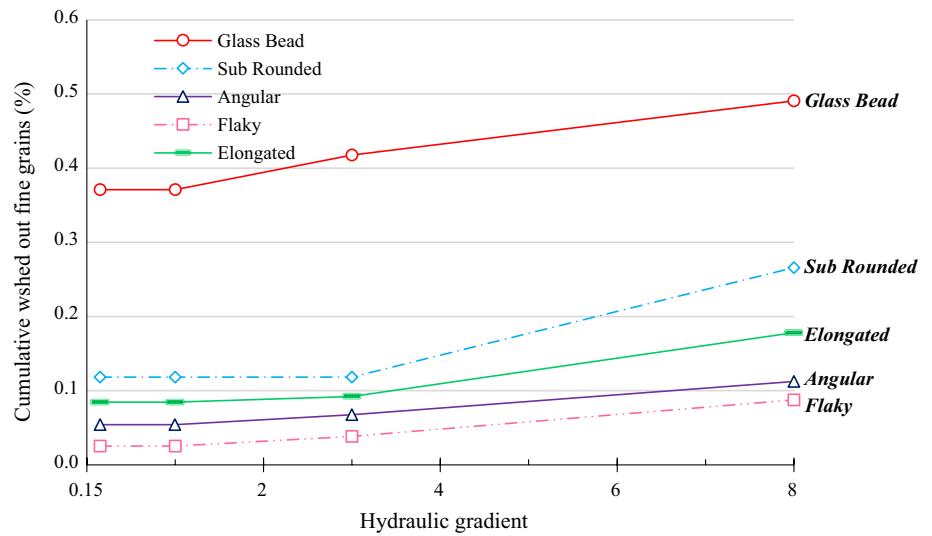


Fig. 7 Percentage of cumulative fines loss after hydraulic gradient for “B” grading

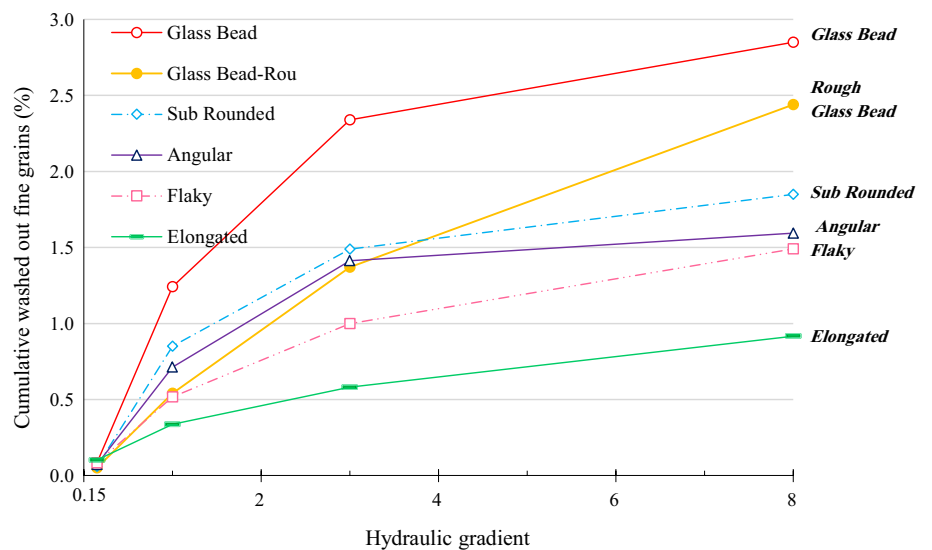


Fig. 8 Percentage of cumulative fines loss after hydraulic gradient for “M1” grading

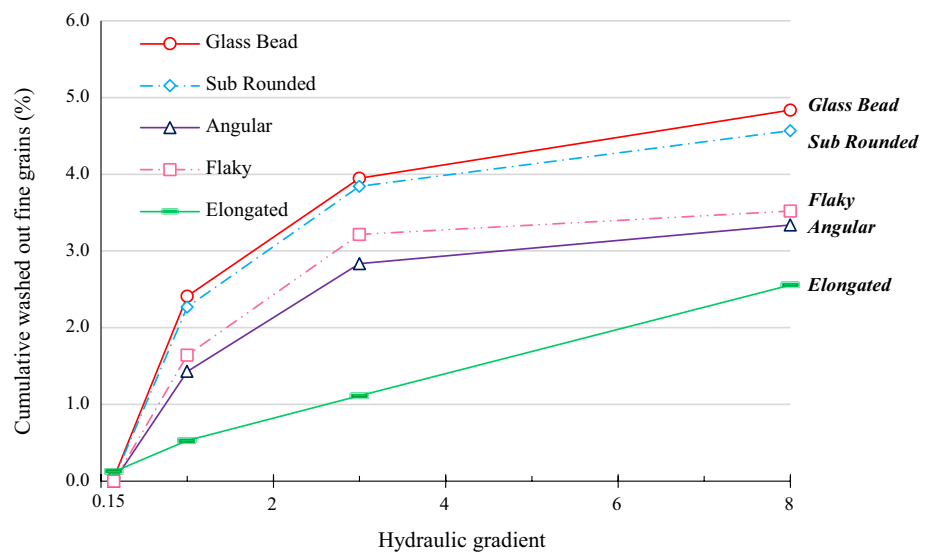
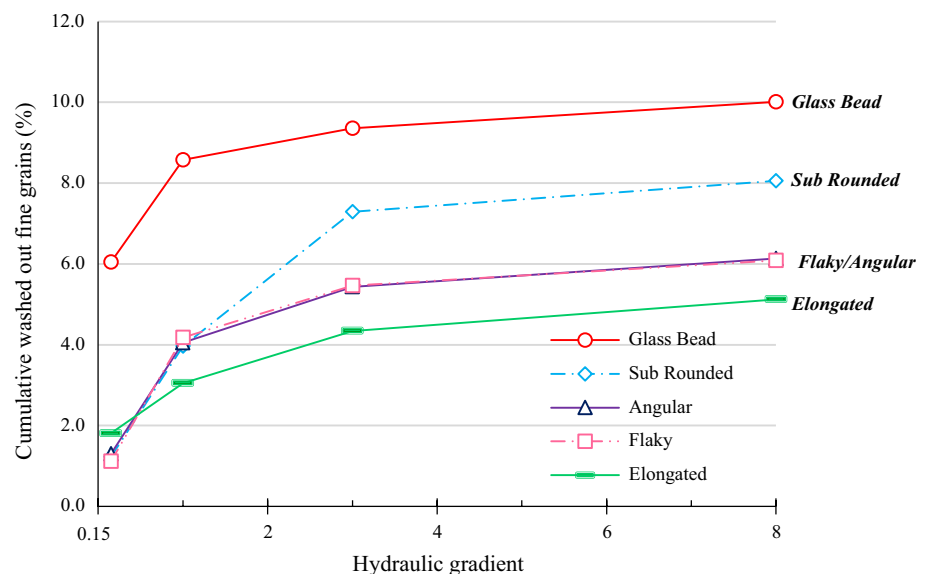


Fig. 9 Percentage of cumulative fines loss after hydraulic gradient for “G3-13” grading



PSD (B and M1) the driving effect is probably coming from particle morphology.

For all the samples of K gradation, no sign of instability was found, and all the samples were internally stable.

According to the test results and visual observations of the sidewall, in the downward flow direction, the B gradation specimen for spherical glass bead, and medium sphericity/rounded particles were suffusive and categorized as internally unstable. Angular and elongated grains were classified as internally stable, and specimens containing flaky grains and rough spherical glass beads were transient.

The M1 samples with glass bead, rounded, crushed, and flaky grains were categorized as a sample with internal instability and suffusion potential. Further, samples with elongated grains were transitional.

All the GP-1 samples except for the elongated grains sample were internally unstable, and the sample with elongated grains was internally stable.

In a reported experiment on G3-13 grading with sample diameter equal to 50 mm and applied hydraulic gradient varying from 0.1 to 6, whereas based on the suffusion classification, it was moderately erodible and classified as unstable by the potential susceptibility classification. This classification takes into account the cumulative mass loss and the expended energy by the fluid flow [48, 49]. In the current study, the total percentage of fraction loss for all the G3-13 samples of this gradation exceeded 3% and entirely were internally unstable (Fig. 9). Further, the specimens with spherical and rounded particles were categorized as suffusive/volume change (Table 8).

Table 8 Summary of obtained the experimental result on different grading with different particle shapes

PSD	Material	Washed out in sidewall	Pipe in sidewall	Max. erosion rate at i_{av} ($g \cdot s^{-1} \cdot m^{-2}$)	Vertical strain (%)	Limit mass loss (%) at i_{av}^{\ddagger}	Su/Vo	Suffusion	Internal stability/instability
K	GB	Moderate	N	1.91 ($i=0.15$) 0.17	–	–	N-S/V	N-Su	S
	R	Relatively High	N	0.51 ($i=0.15$) 0.09	–	–	N-S/V	N-Su	S
	A	No sign	N	0.14 ($i=0.15$) 0.09	–	–	N-S/V	N-Su	S
	F	Moderate	N	0.12 ($i=8.0$) 0.11	–	–	N-S/V	N-Su	S
	E	Moderate	N	0.53 ($i=0.15$) 0.09	–	–	N-S/V	N-Su	S
B	GB	High	BL	3.71 ($i=8.0$) 0.21	–	–	N-S/V	Su	U
	GB- Rou	Moderate	N	2.59 ($i=8.0$) 0.18	–	–	N-S/V	T	T
	R	High	BL	2.61 ($i=8.0$) 0.17	–	–	N-S/V	Su	U
	A	Moderate	N	0.60 ($i=1.0$) 0.09	–	–	N-S/V	N-Su	S
	F	High	BL	1.43 ($i=8.0$) 0.12	–	–	N-S/V	T	T
M1	E	Moderate	N	0.89 ($i=8.0$) 0.09	–	–	N-S/V	N-Su	S
	GB	High	BL	2.78 ($i=3.0$) 0.42	3.95 ($i=3.0$)	N-S/V	Su	U	
	R	High	BL	2.59 ($i=3.0$) 0.13	3.84 ($i=3.0$)	N-S/V	Su	U	
	A	High	BL	3.39 ($i=3.0$) 0.11	3.39 ($i=8.0$)	N-S/V	Su	U	
	F	High	BL	2.03 ($i=3.0$) 0.15	3.52 ($i=8.0$)	N-S/V	Su	U	
GP-1	E	High	BL	2.13 ($i=8.0$) 0.10	–	N-S/V	T	T	
	GB	High	BL& SL	1.71 ($i=1.0$) 1.22	4.33 ($i=0.15$)	S/V	Su	U	
	R	High	BL& SL	2.14 ($i=8.0$) 0.99	5.69 ($i=1.0$)	S/V	Su	U	
	A	High	BL	3.59 ($i=8.0$) 0.37	3.72 ($i=3.0$)	N-S/V	Su	U	
	F	High	BL& SL	1.81 ($i=8.0$) 0.62	4.12 ($i=3.0$)	T	Su	U	
G3-13	E	High	BL	2.25 ($i=8.0$) 0.35	2.97 ($i=8.0$)	N-S/V	T	T	
	GB	High	BL&SL	3.44 ($i=0.15$) 2.89	6.05 ($i=0.15$)	S/V	Su	U	
	R	High	BL&SL	3.78 ($i=3.0$) 1.11	3.97 ($i=1.0$)	S/V	Su	U	
	A	High	BL	2.97 ($i=1.0$) 0.34	4.05 ($i=1.0$)	N-S/V	Su	U	
	F	High	BL	3.13 ($i=1.0$) 0.45	4.18 ($i=1.0$)	N-S/V	Su	U	
E	High	BL	2.45 ($i=3.0$) 0.36	3.05 ($i=1.0$)	N-S/V	Su	U		

GB: Glass bead, GB- Rou: Rough glass bead, R: Rounded particle, A: Angular (Crushed aggregate), F: Flaky (Slate), E: Elongated (Weathered pyramid basalt), Su/Vo: Suffusion/Volume change S: Stable, U: Unstable, T: Transient, Su: Suffusive, N-Su: Non-Suffusive, S/V: Suffusive/Volume change, N-S/V: Non-Suffusive/Volume change, \ddagger) initiation gradient corresponding to the limit mass loss

Fig. 10 Percentage of cumulative fines loss after hydraulic gradient for “GP-1” grading

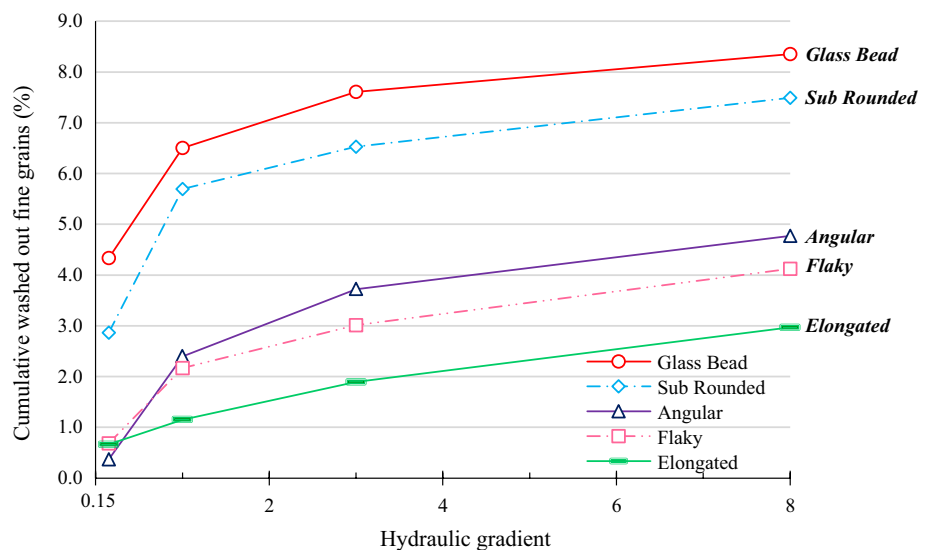


Table 8 illustrates the maximum erosion rate at i_{av} ($\text{g}\cdot\text{s}^{-1}\cdot\text{m}^{-2}$) and limit mass loss (%), corresponding to suffusion susceptibility at i_{av} (initiation hydraulic gradient). Evidently, in soil specimens with similar gradations and different particle shapes suffusion was triggered at an equal or even lower hydraulic gradient.

The suffusion process might affect the soil skeleton and result in the subsidence or development of pipe flow or cracks. It is shown that the development of vertical deformation is strongly dependent on the particle size distribution and particle morphology. For the same gradation, the sample with angular particles with rough texture (crushed and elongated particles), have the minimum vertical strain (see Table 8). Thus, angular particles with the rough surface have more resistance to the suffusion/volume change phenomena.

The comparison of the current experimental results (Table 8) with geometric stability criteria (Table 4) indicates the Istomina (1957) and Kezdi (1979) criteria, prove more conservative for smooth spherical and rounded particles than other methods. Furthermore, Kenney & Lau (1985), Burenkova (1993), Wan & Fell (2008), Li & Fannin (2013), and Chang and Zhang (2013) criteria may be more conservative for low sphericity/rough surface particles.

5.2 Discussion

The current experiment results showed that specimens with various particle shapes have different levels of suffusion or suffusion/volume change. Spherical glass bead and rounded/medium sphericity specimens were more prone to suffusion at an equivalent or even lower hydraulic gradient than the soil samples with angular/low sphericity grains. These results show an agreement with previous research [45]; nevertheless, additional variables should also be considered:

For entire soil samples, an attempt was taken place to keep the factors controlling the internal stability similar and repeatable. These factors include the shape of the PSD curve, relative density, applied gradient, and flow direction. It should be noted that grading is done with square-mesh sieves and is a function of particle projection in 2D. Therefore, the maximum width and thickness control the grading curve shape [66]. Considering the diameter of a sphere circumscribing the grains, diameter of spheres with the same volume as particles, or diameter of spheres with the same surface area as the particles, the shape of the grading curve would be different, especially for flaky and elongated grains [17].

Results indicated that the reduction in the sphericity or roundness of the grains caused the rate of fine grains erosion to be decreased (Fig. 11). The reason could be attributed to the mean pore length reduction [67], increasing the tortuosity, and reduction of constriction sizes can be accompanied by increasing the probability of clogging of the fine grains.

In the samples with flaky and elongated grains, particle arrangement had a higher effect on pore size distribution than samples with rounded or crushed grains. In these samples, the pores network is influenced by the flatness and orientation of grains [68], whether the grains are placed on their largest face, medium face, and smallest face or oriented. In the present work, specimens were prepared in such a way that the grains were placed on the largest face or with a small orientation.

In addition to sphericity and roundness, the particle's roughness can also influence the soil structure and the amount and size of the eroded grains. Constriction size and the coefficient of permeability increase with roughness, whereas, the eventuality of trapping of fine grains in the constriction increases.

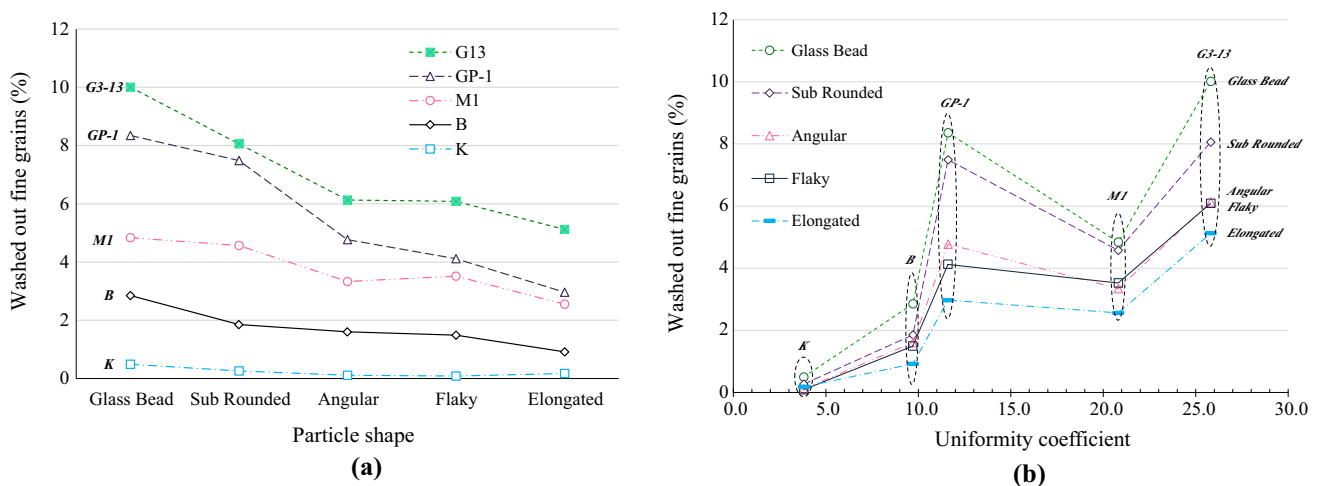


Fig. 11 **a** Total mass loss for samples with different particle shapes, **b** total mass loss for samples with different particle shapes and different uniformity coefficients

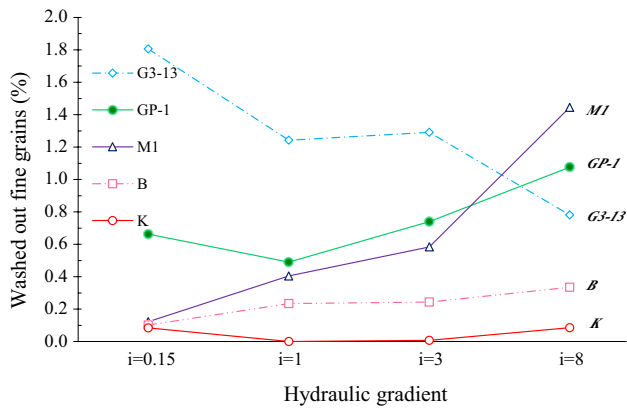


Fig. 12 Percentage of fines loss after each hydraulic gradient for elongated particles

Based on Figs. 7, 8, and 12, there seems to be a quasi-linear relationship between the eroded mass and the hydraulic gradient for the elongated particles. Generally, fine loss rate increases with applied hydraulic gradient, and it was observed that fine particles were eroded in higher hydraulic gradient, compared with smooth spherical glass bead, relatively smooth flaky particles, rough crushed aggregate, and relatively smooth rounded particles, as depicted in Fig. 11. Moreover, the same manner was observed for spherical glass beads with a rough texture in the B gradation (see Fig. 7).

This can be related to the particle sphericity and roughness effects for elongated particles, and roughness for rough spherical glass beads. So, the sphericity and roughness may be controlled the susceptibility to particle migration. As geological evidence, weathering and crushing affect both the surface texture and roundness by exposing fresh surfaces and appearing new corners [50, 69]. Therefore, the particle roughness usually increases with particle angularity [50] and three particle shape characteristics may concurrently affect particle migration.

Surface texture is scale-dependent, and its quantification is difficult. Also, detecting relative contributions of such parameters as roundness, sphericity, and roughness by such individual measurements is not possible [70]. To simplify interpretation, regularity, ρ , is differentiated from an ideal sphere by defining the average of roundness and sphericity, $\rho = \left(\frac{R+S}{2}\right)$, [70].

Roundness is measured in 2D, and sphericity is measured in 3D, and regularity could be a proper estimation of grain morphology. As illustrated in Fig. 13, the percentage of mass loss increases concerning the particle regularity, which is confirmed by a similar amount of mass loss in crushed and flaky samples, which have different shapes but the same regularity (Fig. 13). These results show that

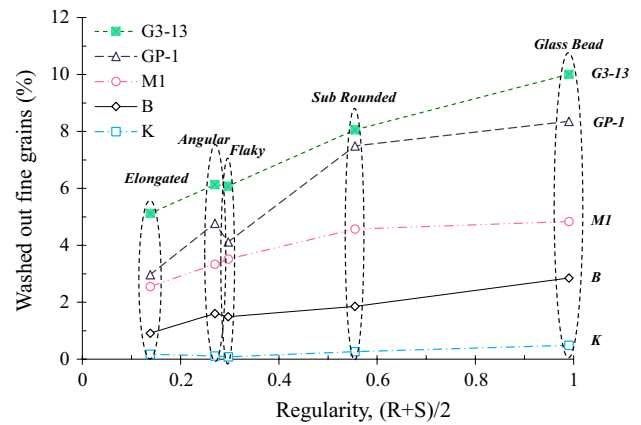


Fig. 13 Effect of particle regularity on washed-out fine grains

the ideal smooth spheres and elongated grains with the rough surface may have the highest and lowest prone to suffusion, respectively.

The shape of finer fraction grains could influence the suffusion phenomenon, as well as the morphology of coarser fraction particles. Decreasing the sphericity and roundness and increased roughness, in addition to the increase in the specific surface area [27], might increase the friction between fine grains and coarser fraction. Therefore, the possibility of finer grain trapping within the pores and clogging increases. It must be noted that further study would be required to validate the effect of surface roughness and finer fraction morphology.

6 Conclusions

Grain morphology is one of the most important parameters affecting the pore geometry and constriction size distribution of soils. In this study, the suffusion test was conducted using different samples with five types of PSD curves and containing the particles with six different shapes to investigate the effect of grain shapes on the internal stability of soil samples.

Gradations were chosen to comprise different shapes of PSD curves and various internal stability conditions, and particle shape was assessed in terms of three features. Sphericity was calculated using 3D images extracted using X-ray micro-computed tomography (μ CT) images. Wadell's roundness was determined using grain projection in 2D. Besides, the surface roughness was described by visual comparison.

Results of suffusion tests showed that grains' morphology effectively changes the seepage flow, mass loss rates, mass loss observed in plexiglas sidewall, and total mass loss. For nearly identical gradations and hydraulic

conditions, the samples with different grain shapes could be internally stable or unstable.

In K gradation, the sample with glass bead and rounded particles had the highest mass loss, and all the samples were internally stable. According to B gradation test results, the glass bead and rounded shape samples were suffusive, and the samples with crushed and elongated grains were internally stable; however, flaky grains were transitional. M1 gradation samples with the glass bead, rounded shape, crushed, and flaky were internally unstable, and elongated grain was transitional. For GP-1 gradation except for the elongated grains sample, which was transitional, all other samples were internally unstable. All G3-13 samples were internally unstable. Further, the sample with glass bead and rounded particles of GP-1 and G3-13 were classified as suffusive/volume change. Meanwhile, samples with the same gradation and different grain shapes were found to have different levels of internal stability/ instability.

Particle regularity could provide a reasonable estimation of grain morphology considering the measurement of grains' roundness in the 2D and sphericity of grains in the 3D. The percentage of fraction loss in all the samples increased with the particle regularity, indicating that ideal smooth spheres and elongated grains with the rough surface may have the highest and lowest prone to suffusion, respectively.

The pipe observed in the permeameter sidewall, the amount of eroded particles, and vertical strain increased with sphericity and roundness of grains (increase in regularity). Subsequently, suffusion and suffusion/volume change were triggered at an equal, or even lower hydraulic gradients in soil specimens with similar gradations and different particle shape.

These results confirm the predictions of relations in the capillary tube model. In these relations, grains' shape coefficient increased with the grains' angularity and mean diameter of pores, and consequently, the amount of eroded grain also reduced. This study mainly aimed to investigate the effect of particle morphology on suffusion susceptibility of granular soils. Arguably, many contributing factors are involved in the internal stability of soils, such as relative density, particle arrangement, applied stress, and flow direction that are beyond the scope of this research as well as proposing a model based on quantitative multivariate analysis. More experimental results in order to form a comprehensive database are required and providing a simple practical approach for practitioners can be a future perspective.

Compliance with ethical standards

Conflict of interest The authors declare that they have no conflict of interest.

References

1. Foster, M., Fell, R., Spannagle, M.: The statistics of embankment dam failures and accidents. *Can. Geotech. J.* **37**, 1000–1024 (2000). <https://doi.org/10.1139/t00-030>
2. ICOLD: Internal erosion of existing dams, levees and dikes, and their foundations. *Bull.*, 1: 342 (2015)
3. Kenney, T.C., Lau, D.: Internal stability of granular filters. *Can. Geotech. J.* **22**, 215–225 (1985). <https://doi.org/10.1139/t86-068>
4. Shire, T., O'Sullivan, C., Hanley, K.J.: The influence of fines content and size-ratio on the micro-scale properties of dense bimodal materials. *Granul. Matter.* **18**, (2016). <https://doi.org/10.1007/s10035-016-0654-9>
5. Taha, H., Nguyen, N.-S., Marot, D., Hijazi, A., Abou-Saleh, K.: Micro-scale investigation of the role of finer grains in the behavior of bidisperse granular materials. *Granul. Matter.* **21**, 28 (2019). <https://doi.org/10.1007/s10035-019-0867-9>
6. Douglas, K.J., Fell, R., Peirson, W.L., Studholme, H.: Experimental investigation of global backward erosion and suffusion of soils in embankment dams. *Can. Geotech. J.* **56**, 789–807 (2019). <https://doi.org/10.1139/cgj-2018-0088>
7. Chapuis, R.P., Saucier, A.: Assessing internal erosion with the modal decomposition method for grain size distribution curves. *Acta Geotech.* **15**(6), 1595–1605 (2019). <https://doi.org/10.1007/s11440-019-00865-z>
8. Marot, D., Benamar, A.: Suffusion, Transport and Filtration of Fine Particles in Granular Soil. In: Bonelli, S. (ed.) *Erosion of Geomaterials*, pp. 39–79. John Wiley & Sons Inc, Hoboken, NJ, USA (2013)
9. Fannin, R.J., Slangen, P.: On the distinct phenomena of suffusion and suffosion. *Géotechnique Lett.* **4**, 289–294 (2014). <https://doi.org/10.1680/geolett.14.00051>
10. Richards, K.S., Reddy, K.R.: Critical appraisal of piping phenomena in earth dams. *Bull. Eng. Geol. Environ.* **66**, 381–402 (2007). <https://doi.org/10.1007/s10064-007-0095-0>
11. USBR-USACE: Best practices in dam and levee safety risk analysis, Technical Report Version 4.0. , US Bureau of Reclamation and the US Army Corps of Engineers, Denver, CO, USA (2015)
12. Hunter, R.P., Bowman, E.T.: Visualisation of seepage-induced suffusion and suffosion within internally erodible granular media. *Géotechnique.* **68**, 918–930 (2018). <https://doi.org/10.1680/jgeot.17.P.161>
13. Aboul Hosn, R., Sibille, L., Benahmed, N., Chareyre, B.: A discrete numerical model involving partial fluid-solid coupling to describe suffusion effects in soils. *Comput. Geotech.* **95**, 30–39 (2018). <https://doi.org/10.1016/j.compgeo.2017.11.006>
14. Scholtès, L., Hicher, P.-Y., Sibille, L.: Multiscale approaches to describe mechanical responses induced by particle removal in granular materials. *Comptes Rendus Mécanique.* **338**, 627–638 (2010). <https://doi.org/10.1016/j.crme.2010.10.003>
15. Aberg, B.: Void sizes in granular soils. *J. Geotech. Eng.* **122**, 236–239 (1996). [https://doi.org/10.1061/\(ASCE\)0733-9410\(1996\)122:3\(236\)](https://doi.org/10.1061/(ASCE)0733-9410(1996)122:3(236))
16. Shire, T., O'Sullivan, C.: Micromechanical assessment of an internal stability criterion. *Acta Geotech.* **8**, 81–90 (2013). <https://doi.org/10.1007/s11440-012-0176-5>
17. Kezdi, A.: *Soil Physics- Selected Topics*. Elsevier, Amsterdam (1979)
18. Wan, C.F., Fell, R.: Assessing the Potential of Internal Instability and Suffusion in Embankment Dams and Their Foundations. *J. Geotech. Geoenviron. Eng.* **134**, 401–407 (2008). [https://doi.org/10.1061/\(ASCE\)1090-0241\(2008\)134:3\(401\)](https://doi.org/10.1061/(ASCE)1090-0241(2008)134:3(401))
19. Salehi Sadaghiani, M.R., Witt, K.J.: Experimental identification of mobile particles in suffusible non cohesive soils.

- Eur. J. Environ. Civ. Eng. **15**, 1155–1165 (2011). <https://doi.org/10.1080/19648189.2011.9714846>
20. Seghir, A., Benamar, A., Wang, H.: Effects of fine particles on the suffusion of cohesionless soils. *Exp. Model. Transp. Porous Media*. **103**, 233–247 (2014). <https://doi.org/10.1007/s11242-014-0299-2>
 21. Zhong, C., Le, V.T., Bendahmane, F., Marot, D., Yin, Z.: Investigation of spatial scale effects on suffusion susceptibility. *J. Geotech. Geoenviron. Eng.* **144**, 04018067 (2018). [https://doi.org/10.1061/\(ASCE\)GT.1943-5606.0001935](https://doi.org/10.1061/(ASCE)GT.1943-5606.0001935)
 22. Chapuis, R.P.: Similarity of internal stability criteria for granular soils. *Can. Geotech. J.* **29**, 711–713 (1992). <https://doi.org/10.1139/t92-078>
 23. Kovács, G.: *Seepage Hydraulics*, Elsevier, Amsterdam (1981)
 24. Kenney, T.C., Chahal, R., Chiu, E., Ofoegbu, G.I., Omange, G.N., Ume, C.A.: Controlling constriction sizes of granular filters. *Can. Geotech. J.* **22**, 32–43 (1985). <https://doi.org/10.1139/t85-005>
 25. Aberg, B.: Washout of grains from filtered sand and gravel materials. *J. Geotech. Eng.* **119**, 36–53 (1993). [https://doi.org/10.1061/\(ASCE\)0733-9410\(1993\)119:1\(36\)](https://doi.org/10.1061/(ASCE)0733-9410(1993)119:1(36))
 26. Seblany, F., Homberg, U., Vincens, E., Winkler, P., Josef Witt, K.: Merging criteria for defining pores and constrictions in numerical packing of spheres. *Granul. Matter.* **20**, 37 (2018). <https://doi.org/10.1007/s10035-018-0808-z>
 27. Maroof, M.A., Mahboubi, A., Noorzad, A.: A new method to determine specific surface area and shape coefficient of a cohesionless granular medium. *Adv. Powder Technol.* **31**, 3038–3049 (2020). <https://doi.org/10.1016/j.apt.2020.05.028>
 28. Istomina, V. S.: Filtration stability of soils. In: *Oostroizdat*, Moscow, Leningrad (in Russian) (1957)
 29. Kenney, T.C., Lau, D.: Internal stability of granular filters: Reply. *Can. Geotech. J.* **23**, 420–423 (1986). <https://doi.org/10.1139/t86-068>
 30. Burenkova, V. V.: Assessment of the internal instability for granular soils subjected to seepage. In: *1st international conference, Filters in geotechnical and hydraulic engineering*. pp. 357–360. Balkema, Karlsruhe; Germany (1993)
 31. Chang, D.S., Zhang, L.M.: Extended internal stability criteria for soils under seepage. *Soils Found.* **53**, 569–583 (2013). <https://doi.org/10.1016/j.sandf.2013.06.008>
 32. Skempton, A.W., Brogan, J.M.: Experiments on piping in sandy gravels. *Géotechnique*. **44**, 449–460 (1994). <https://doi.org/10.1680/geot.1994.44.3.449>
 33. Sibille, L., Marot, D., Sail, Y.: A description of internal erosion by suffusion and induced settlements on cohesionless granular matter. *Acta Geotech.* **10**, 735–748 (2015). <https://doi.org/10.1007/s11440-015-0388-6>
 34. Adel, H.D., Bakker, K.J., Breteler, M.K.: Internal stability of minestone. In: *International Symposium on Modelling Soil–Water–Structure Interactions*. p. 225–231. , Balkema, Rotterdam (1988)
 35. Salehi, M., Witt, K., Odenwald, B.: Experimental investigations of critical hydraulic gradients for a soil prone to suffusion. In: *Scour and Erosion*. pp. 1033–1043. CRC Press, Taylor & Francis Group, 6000 Broken Sound Parkway NW, Suite 300, Boca Raton, FL 33487–2742 (2016)
 36. Andrianatrehina, L., Souli, H., Rech, J., Taibi, S., Fry, J.-J., Bunieski, S., Fleureau, J.-M.: Determination of the maximum diameter of free fines to assess the internal stability of coarse granular materials. *Eur. J. Environ. Civ. Eng.* **21**, 332–347 (2017). <https://doi.org/10.1080/19648189.2015.1116468>
 37. Moffat, R.: Experiment on the internal stability of widely graded cohesionless soils, (2005)
 38. Li, S., Russell, A.R., Muir Wood, D.: Influence of particle-size distribution homogeneity on shearing of soils subjected to internal erosion. *Can. Geotech. J.* **57**, 1684–1694 (2020). <https://doi.org/10.1139/cgj-2019-0273>
 39. Moffat, R., Fannin, R.J., Garner, S.J.: Spatial and temporal progression of internal erosion in cohesionless soil. *Can. Geotech. J.* **48**, 399–412 (2011). <https://doi.org/10.1139/T10-071>
 40. Slangen, P.: On the influence of effective stress and micro-structure on suffusion and suffosion, PhD thesis, The university of British Columbia, (2015)
 41. Li, M., Fannin, R.J.: Capillary Tube Model for Internal Stability of Cohesionless Soil. *J. Geotech. Geoenviron. Eng.* **139**, 831–834 (2013). [https://doi.org/10.1061/\(ASCE\)GT.1943-5606.0000790](https://doi.org/10.1061/(ASCE)GT.1943-5606.0000790)
 42. Indraratna, B., Vafai, F.: Analytical Model for Particle Migration within Base Soil-Filter System. *J. Geotech. Geoenviron. Eng.* **123**, 100–109 (1997).
 43. Dallo, Y.A.H., Wang, Y.: Determination of controlling constriction size from capillary tube model for internal stability assessment of granular soils. *Soils Found.* **56**, 315–320 (2016). <https://doi.org/10.1016/j.sandf.2016.02.013>
 44. Marot, D., Bendahmane, F., Haï Nguyen, H.: Influence of angularity of coarse fraction grains on internal erosion process. *La Houille Blanche* **6**, 47–53 (2012)
 45. Slangen, P., Fannin, R.J.: The role of particle type on suffusion and suffosion. *Géotechnique Lett.* **7**, 6–10 (2017). <https://doi.org/10.1680/jgele.16.00099>
 46. Crawford-Flett, K.: An improved hydromechanical understanding of seepage-induced instability phenomena in soil. PhD thesis, The University of British Columbia, Vancouver, Canada (2014)
 47. Sail, Y., Marot, D., Sibille, L., Alexis, A.: Suffusion tests on cohesionless granular matter. *Eur. J. Environ. Civ. Eng.* **15**, 799–817 (2011). <https://doi.org/10.1080/19648189.2011.9693366>
 48. Marot, D., Rochim, A., Nguyen, H.H., Bendahmane, F., Sibille, L.: Assessing the susceptibility of gap-graded soils to internal erosion: proposition of a new experimental methodology. *Nat. Hazards*. **83**, 365–388 (2016). <https://doi.org/10.1007/s11069-016-2319-8>
 49. Le, V.T., Marot, D., Rochim, A., Bendahmane, F., Nguyen, H.H.: Suffusion susceptibility investigation by energy-based method and statistical analysis. *Can. Geotech. J.* **55**, 57–68 (2018). <https://doi.org/10.1139/cgj-2017-0024>
 50. Barrett, P.J.: The shape of rock particles, a critical review. *Sedimentology*. **27**, 291–303 (1980)
 51. Mitchell, J., Soga, K.: *Fundamentals of soil behavior*. Wiley, New York (2005)
 52. Suhr, B., Six, K.: Simple particle shapes for DEM simulations of railway ballast: influence of shape descriptors on packing behaviour. *Granul. Matter.* **22**, 43 (2020). <https://doi.org/10.1007/s10035-020-1009-0>
 53. Su, Y.F., Lee, S.J., Sukumaran, B.: Influence of particle morphology simplification on the simulation of granular material behavior. *Granul. Matter.* **22**(1), 1–12 (2020)
 54. ASTM D2488–09a: Standard Practice for Description and Identification of Soils (Visual-Manual Procedure). ASTM Int. West Conshohocken, PA., (2009). <https://doi.org/10.1520/D2488-09A>
 55. Maroof, M.A., Mahboubi, A., Noorzad, A., Safi, Y.: A new approach to particle shape classification of granular materials. *Transp. Geotech.* **22**, 100296 (2020). <https://doi.org/10.1016/j.trge.2019.100296>
 56. Wadell, H.: Volume, Shape, and Roundness of Rock Particles. *J. Geol.* **40**, 443–451 (1932). <https://doi.org/10.1086/623964>
 57. Powers, M.C.: A New Roundness Scale for Sedimentary Particles. *SEPM J. Sediment. Res.* **23**, 117–119 (1953). <https://doi.org/10.1306/D4269567-2B26-11D7-8648000102C1865D>
 58. Nguyen, C.D., Benahmed, N., Andò, E., Sibille, L., Philippe, P.: Experimental investigation of microstructural changes in soils eroded by suffusion using X-ray tomography. *Acta Geotech.* **14**, 749–765 (2019). <https://doi.org/10.1007/s11440-019-00787-w>

59. Moffat, R., Fannin, R.: A Large Permeameter for Study of Internal Stability in Cohesionless Soils. *Geotech. Test. J.* **29**, 273–279 (2006). <https://doi.org/10.1520/GTJ100021>
60. Ke, L., Takahashi, A.: Experimental investigations on suffusion characteristics and its mechanical consequences on saturated cohesionless soil. *Soils Found.* **54**, 713–730 (2014). <https://doi.org/10.1016/j.sandf.2014.06.024>
61. Head, K.H., Epps, R.: *Manual of Soil Laboratory Testing—Volume 2: Permeability. Shear Strength and Compressibility Tests*, Whittles Publishing (2011)
62. SanthanaKrishnan, N., Neelakantan, T.R.: Analysis of susceptibility to suffusion. *ARNP J. Eng. Appl. Sci.* **9**, 1999–2008 (2014)
63. Rochim, A., Marot, D., Sibille, L., Le Thao, V.: Effects of Hydraulic Loading History on Suffusion Susceptibility of Cohesionless Soils. *J. Geotech. Geoenviron. Eng.* **143**, 04017025 (2017). [https://doi.org/10.1061/\(ASCE\)GT.1943-5606.0001673](https://doi.org/10.1061/(ASCE)GT.1943-5606.0001673)
64. Luo, Y. L., Qiao, L., Liu, X. Xing, Zhan, M. li, Sheng, J. chang: Hydro-mechanical experiments on suffusion under long-term large hydraulic heads. *Nat. Hazards.* **65**: 1361–1377 (2013)
65. Chapuis, R.P.: Predicting the saturated hydraulic conductivity of sand and gravel using effective diameter and void ratio. *Can. Geotech. J.* **41**, 787–795 (2004). <https://doi.org/10.1139/t04-022>
66. Allen, T.: *Particle Size Measurement*. Springer, US, Boston, MA (1981)
67. Van Lopik, J.H., Snoeijers, R., Van Dooren, T.C.G.W., Raoof, A., Schotting, R.J.: The effect of grain size distribution on nonlinear flow behavior in sandy porous media. *Transp. Porous Media.* **120**, 37–66 (2017). <https://doi.org/10.1007/s11242-017-0903-3>
68. Witt, K.-J., Brauns, J.: Permeability-Anisotropy Due to Particle Shape. *J. Geotech. Eng.* **109**, 1181–1187 (1983). [https://doi.org/10.1061/\(ASCE\)0733-9410\(1983\)109:9\(1181\)](https://doi.org/10.1061/(ASCE)0733-9410(1983)109:9(1181))
69. Krumbein, W.C.: The effects of abrasion on the size, shape and roundness of rock fragments. *J. Geol.* **49**, 482–520 (1941). <https://doi.org/10.1086/624985>
70. Cho, G.-C., Dodds, J., Santamarina, J.C.: Particle Shape Effects on Packing Density, Stiffness, and Strength: Natural and Crushed Sands. *J. Geotech. Geoenviron. Eng.* **132**, 591–602 (2006). [https://doi.org/10.1061/\(ASCE\)1090-0241\(2006\)132:5\(591\)](https://doi.org/10.1061/(ASCE)1090-0241(2006)132:5(591))

Publisher's Note Springer Nature remains neutral with regard to jurisdictional claims in published maps and institutional affiliations.